ICAS 2016
30th Congress of the International Council of the Aeronautical Sciences
DCC, Daejeon, Korea ; September 25-30, 2016

MULTI-OBJECTIVE OPTIMAL DESIGN OF THE PROPELLER FOR HIGH ALTITUDE AIRSHIPS BASED ON HIGH EFFICIENCY AND LIGHT WEIGHT

Jun Jiao*, Yu-Gang Zhang, Bi-Feng Song
*** School of Aeronautics, Northwestern Polytechnical University, Xi'an, China**

Keywords: *optimal design, high altitude, propeller, nsga-ii, experiment*

Abstract

In order to make full use of the power of engine and reduce the energy consumption, propeller need to be highly efficient and lightweight to satisfy the High Altitude Airship's (HAA) requirements during the high altitude and long endurance flight period. This paper presents a multi-objective optimization design method of the propeller for HAA. The vortex theory is used to predict the propeller's aerodynamic performance and the non-dominated sorting genetic algorithm II (NSGA-II) is applied to solve the optimization problem. Then the optimization model which has two objectives of high efficiency and light weight of the propeller is established according to the conditions of the HAA's propulsion system. In addition, the effects of the various parameters including pitch angle, chord width, rotational speed and diameter on high altitude propeller performance are discussed in detail. In order to evaluate the performance of the optimized propeller, wind tunnel experiment of scale model based on scaling laws was carried out and the numerical results are validated to be agreed reasonably well with the two experimental data.

1 Introduction

In recent years, the great potential for the use of lighter than air (LTA) platforms for military and civilian applications has been reassessed in many aviation developed countries [1, 2]. In particular, due to the extended duration of time (months to years) at high altitudes (18km and higher), HAA is considered as an excellent platform for many different purposes in both civil and military fields such as aerial exploration, communications support, intelligence, surveillance, and reconnaissance (ISR) or even as a solution for aerial transportation [3, 4].

One of the most efficient ways for a low speed airship to generate thrust within a very low Reynolds number flight regime is propeller. Moreover, the performance of the propeller directly affect the size of the power system as well as the other propulsion system components of the whole HAA. Therefore, the classic problem of high altitude propeller design has been and remains a topic of considerable interest [5]. In reality, the design of the propeller based on minimum induced losses started with Betz and Goldstein in the beginning of the 20th century and then developed by a variety of excellent scientist for more than a century [6]. These numerical methods are still utilized in the design of high altitude propellers, and play a significant role in the preliminary design of HAA propulsion system [7-9]. In addition, considering the complex surface shape and structure of the composite propeller blades, it would be very difficult to obtain the blade weight, therefore a numerical model that transforms the weight of the blade into its surface area is an effective approach [10].

In this study, a method for predicting the aerodynamic performance and weight is integrated into the multi-objective optimization design of high altitude propeller. Based on the vortex theory and the NSGA-II algorithm, a mathematical model which maximizes the efficiency and minimizes the blade area of propeller blades is established. Then the effects of the design variables, including pitch angle, chord width, rotational speed and diameter on high altitude propeller performance and weight are discussed in detail. At last, scale model

experiment of the optimal propeller was carried out in the wind tunnel according to the scaling laws, the performance of the designed propeller are obtained and compared.

2 Propeller Performance Calculation

In order to quantitatively predict the performance of a rotating propeller, the aerodynamics of the blade need to be analyzed in detail [11]. To this end, the cross-section of the propeller blade is shown in Fig. 1. The propeller is rotating with a rotational speed of ns and advancing through the air with velocity of V. The pitch angle, β, is defined relative to the zero lift line of the airfoil section which varies with the radial distance r. Similar to finite wing theory, the total down wash angle, θ, is the sum of two parts, the advanced angle, φ, and induced angle of attack resulting from the induced velocity ω, α_i., the contribution of one-blade element to the thrust, dT, and torque, dQ, are related to the differential lift and drag forces,

$$dT = \tfrac{1}{2}\rho V_E^2 c[C_l \cos(\varphi+\alpha_i) - C_d \sin(\varphi+\alpha_i)]dr \quad (1)$$

$$dQ = \tfrac{1}{2}\rho V_E^2 c[C_l \sin(\varphi+\alpha_i) + C_d \cos(\varphi+\alpha_i)]rdr \quad (2)$$

The section lift and drag coefficient, C_l and C_d, depend on the local Reynolds and Mach number, Re and Ma, and aerodynamic angle of attack for the blade element, α. From the tangential and axial component of induced velocity, ω_t and ω_a, the angle of attack α be determined as

$$\alpha = \beta - \varphi - \alpha_i = \beta - \tan^{-1}\left(\frac{V+\omega_a}{2\pi n_s r - \omega_t}\right) \quad (3)$$

And the induced angle can also be determined easily from the same geometry as

$$\alpha_i = \theta - \varphi = \tan^{-1}\left(\frac{V+\omega_a}{2\pi n_s r - \omega_t}\right) - \tan^{-1}\left(\frac{V}{2\pi n_s r}\right) \quad (4)$$

From the geometry shown in Fig. 1, the resultant relative velocity, V_E, at the plane of the blade is given by

$$V_E = \sqrt{(V+\omega_a)^2 + (2\pi n_s r - \omega_t)^2} \quad (5)$$

The Kutta-Joukowski theorem states that the lift on a finite propeller blade is related to the bound vorticity through the vortex lifting law. Thus, the local section circulation, Γ, can be expressed as

$$\Gamma = \tfrac{1}{2} c C_l V_E \quad (6)$$

According to Goldstein's vortex theory, the induced velocity is assumed to be normal to the resultant velocity, thus the two parts of the induced velocity are related by

$$\frac{V+\omega_a}{2\pi n_s r - \omega_t} = \frac{\omega_t}{\omega_a} \quad (7)$$

Goldstein related ω_t in the plane of the propeller disk bound to the local section circulation via Eq. (13).

$$B\Gamma = 4\pi r \kappa \omega_t \simeq 4\pi r F \omega_t \quad (8)$$

The Goldstein's kappa factor, κ, which is difficult to find a numerical solution, is replaced by Prandtl's tip loss factor, F. It is expressed as

$$F = \frac{2}{\pi}\cos^{-1}\left\{\exp\left[-\frac{B(1-2r/d)}{2\sin\beta_t}\right]\right\} \quad (9)$$

where d is the diameter of the propeller, B is the number of blades and β_t is the pitch angle at the propeller blade tip.

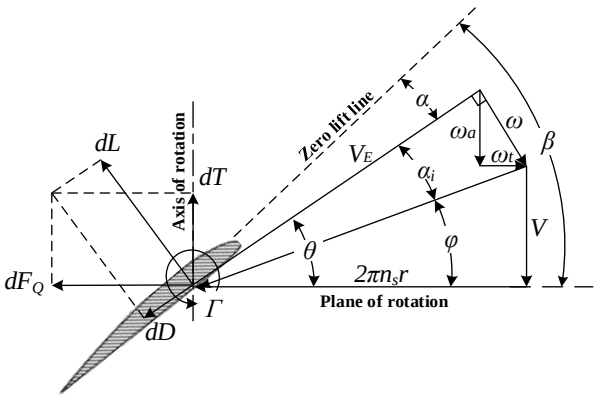

Fig. 1. Section forces and velocities acting on a rotating propeller blade

According to the blade element theory, several variables including β, V, $n_s r$, c, H, Y, are influential to the aerodynamic characteristics of the blade element. These parameters and their relationships associated with the lift and drag coefficients of the blade section is shown in Fig. 2. It is shown that the performance of a certain airfoil with the change of α is only related with different Reynolds and Mach numbers. In addition, XFOIL has proven to be a powerful and very useful tool for the design and analysis of the airfoil aerodynamic characteristics at low-speed and low Reynolds numbers [12, 13]. Therefore, the correspondence between C_l, C_d and α can be fitted by polynomial spines and

calculated by XFOIL with different Reynolds and Mach numbers.

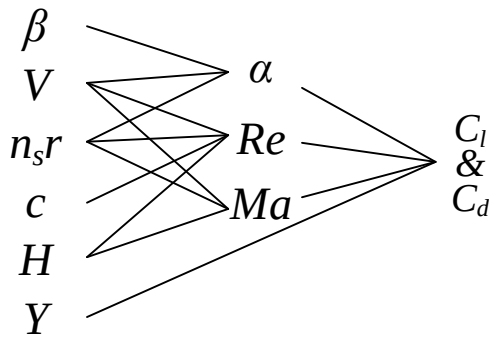

Fig. 2 Relationship of the parameters associated with blade element aerodynamics

Given the propeller blade geometry and operating condition of the blade section, the iteration for α_i proceeds as outlined below:

1. Assume ω_t=0, the initial value of α_i can be obtained through Eq. (4) and Eq. (7).
2. α calculated from Eq. (3).
3. C_l, C_d from XFOIL with certain *Re* and *Ma*.
4. V_E calculated from Eq. (5).
5. Γ calculated from Eq. (6).
6. ω_t, ω_a calculated from Eqs. (7~9)
7. α_i calculated from Eq. (4)

The result from step 7 is then returned to step 2 until the absolute difference between the calculated value of α_i and that from the previous calculation reduces to a desired value (like 0.00001 rad).

Then *dT* and *dQ* of each section are uniquely determined as Eqs. 1 and 2. Ultimately the thrust and torque on the overall propeller can be computed by integrating the differential quantities from the hub diameter to the tip diameter.

3 Blade Weight Estimation Method

High altitude propeller is usually made of composite materials. The blade density varies greatly with the different lamination design. It would be very difficult to obtain the blade weight by using composite laminate theory. Thus, weight estimation of the propeller is simplified as blade surface area calculation to avoid building structure model of composite propeller blade with different density distribution and complex surface shape, and the estimation method is shown in Fig. 3 [10].

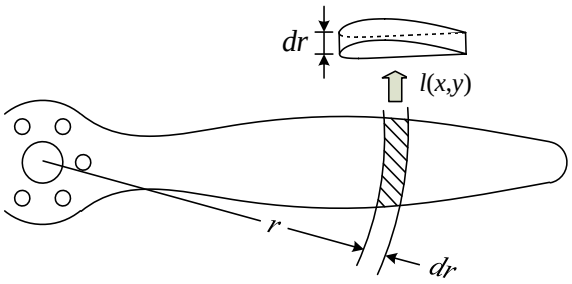

Fig. 3. Method of estimating the blade surface area

The blade area is obtained by numerical spanwise integration of the length for each section profile, as shown in Eq. (15),

$$S = B\lim_{dr\to 0}\sum \Delta S = B\int_{r=r_h}^{r_t} l(x,y)dr \qquad (10)$$

where $l(x, y)$ is the length equation of the blade profile, (x_{i0}, y_{i0}) the airfoil coordinates of unit chord, (x_i, y_i) the transformed airfoil coordinate of the propeller blade.

The length of the blade profile is defined as the limit of the lengths of the inscribed polygons with vertices.

$$l(x,y)=\sum_{i=1}^{n}\sqrt{(x_{i+1}-x_i)^2+(y_{i+1}-y_i)^2} \qquad (11)$$

$$\begin{cases} x_i = c(x_{i0}\cos\beta + y_{i0}\sin\beta) \\ y_i = c(y_{i0}\cos\beta - x_{i0}\sin\beta) \end{cases} \qquad (12)$$

4 Optimal Design of High Altitude Propeller

4.1 Optimization mathematical model

4.1.1 Objective Function

The ability of HAA to an extended duration of time at high altitudes requires an efficient propulsion system. Therefore, the propeller systems of HAA need to be highly efficient and lightweight. So the two objectives are defined as below.

$$Objectives:\ f_1(x)=\max(\eta),\quad f_2(x)=\min(S) \qquad (13)$$

The aerodynamic efficiency of the propeller is defined as the propulsive power, P_p, divided and by the brake power, P, which will be calculated based on the vortex theory.

$$\eta = \frac{P_p}{P} = \frac{TV}{Q2\pi n_s R} = \frac{C_T \lambda}{C_P} \tag{14}$$

Using Eqs. (10) to (12), the blade surface area of the propeller can be obtained through arc length integration.

4.1.2 Design Variables and Constraints

The propeller blade geometry and operating conditions determines the aerodynamic efficiency of the propeller. The high-lift airfoil series self-developed are used in this case, and the position of these airfoils are also previously determined. The relative thickness of the blade airfoil arrangement decreases monotonically from the blade root to the tip. The Airfoil of typical profiles across the blade and their polars are presented in Fig. 4 and 5.

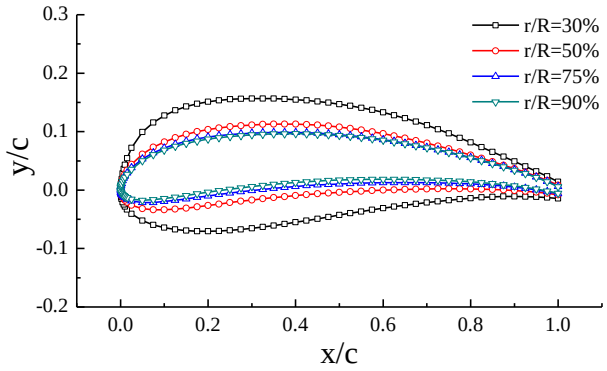

Fig. 4. Airfoil geometries of several sections across the blade

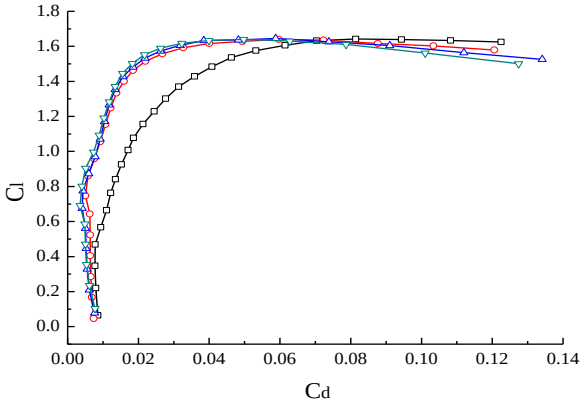

Fig. 5. Airfoil performance in XFOIL for Re=5.00×105 and Ma=0.1

Besides the cross-sectional airfoil, the geometry of the propeller blade are mainly determined by distribution of chord and pitch angle. In order to make the blade smooth and continuous along the spanwise direction, the cubic Bézier curve is used to describe the blade chord and the pitch angle distribution [14],

$$c(x) = (1-x)^3 c_0 + 3x(1-x)^2 c_1 + 3x^2(1-x)c_2 + x^3 c_3 \tag{15}$$

$$\beta(y) = (1-y)^3 \beta_0 + 3y(1-y)^2 \beta_1 + 3y^2(1-y)\beta_2 + y^3 \beta_3 \tag{16}$$

where c_0, c_1, c_2, c_3 represents four control points of the chord distribution, one at hub, one at tip and two at intermediate stations, β_0, β_1, β_2, β_3 represents that of the pitch angel distribution, x, y changes in [0, 1], the range of eight parameters are limited as follows,

$$c_{i\min} \le c_i \le c_{i\max} \quad \beta_{i\min} \le \beta_i \le \beta_{i\max} \quad \text{i=0,…,3} \tag{17}$$

Aside from the geometry (airfoil and blade twist) of the propeller blade, the propeller's diameter and the number of blades are important factors which will significantly affect the performance of the propeller at a given altitude. In addition, in order to take into account the performance of the drive motor, the range of values for rotational speed should be subject to a reasonable limitation as a design variable. Thus, the design variables and their bounds are described in Table 1.

Table 1. Design variables and their ranges

Design variable	Description	Range
C_0	The control parameters of chord distribution, m	0.1~0.6
C_1		0.2~1.0
C_2		0.2~1.0
C_3		0.1~0.6
β_0	The control parameters of pitch angle distribution, degree	20~60
β_1		20~60
β_2		1~30
β_3		1~30
d	Propeller's diameter, m	6.2, 6.8, 7.4
n_s	Propeller's rotational speed, rpm	500~600

Besides the geometrical dimension constraint, several important constraints are applied here to satisfy the performance of the propeller for HAA. The required thrust under the flight condition and the rated power absorbed from the motor are both restricted based on the task requirement and propulsion system of HAA. Because the diameter and rotational speed are both changing during the design process, the tip Mach number defined in Eq. (20) of the propeller must be limited around 0.7 Mach which is easy to be achieved under high altitude and low density environment [15]. This is done to avoid the formation of shock waves on the propeller blade which can severely reduce its performance if not destroy the propeller.

$$Ma_{tip} = \frac{\sqrt{V^2 + (\pi n_s d)^2}}{a} \tag{18}$$

$$Constrants: T \geq T_{\min},\ P_b = P_{rated},\ Ma_{tip} \leq Ma_{\max} \tag{19}$$

The equality and inequality constraints according to the requirements of the HAA propulsion system are summarized in Table 2.

Table 2. Design constraints

Constraint	Description	Value
H	Flight altitude, km	20
V	Wind velocity, m/s	20
B	Number of blades	2
T	Thrust of propeller, N	≥900
P	Propeller absorbed power, kw	25.5
Ma_{tip}	Mach number of the blade tip	≤0.7

4.2 NSGA-II Algorithm

NSGA-II developed by Deb in 2002 is one of the contemporary multi-objective evolutionary algorithms that exhibits high performance and has been widely used in solving MOPs. The algorithm is an improved version of NSGA [16], which applies the fast non-dominated sorting technique and a crowding distance to rank and select the population fronts. Then, the algorithm applies simulated binary crossover (SBX) and polynomial mutation to combine the current population and its offspring generated as next generation. After that a binary tournament selection with crowed comparison-operator is used to rank and select the population fronts. Finally, the best individuals based on non-dominance and elitism are selected as the Pareto optimal solutions [17]. The Procedure of NSGA-II algorithm is shown in Fig. 6.

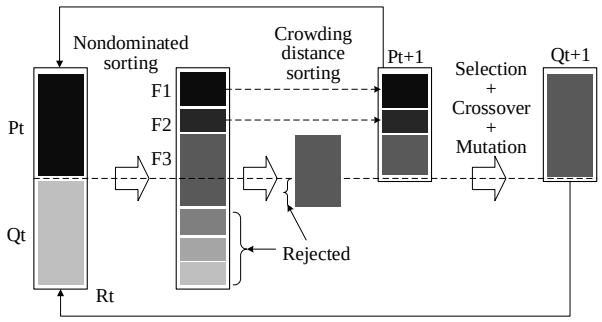

Fig. 6. Schematic of NSGA- II algorithm

4.3 Multi-Objective Optimization

The optimization results of the two-bladed propeller with 6.8-meter diameter are shown in Fig. 7. The optimal region is divided into two parts by the Pareto frontier, part I is an ideal solution region that cannot be reached under the design conditions, while part II is a feasible solution region. The monotonicity of the Pareto frontier shows that the increase of the propeller efficiency is accompanied by the increase of the blade weight, indicating that the two design goals have a certain degree of conflict.

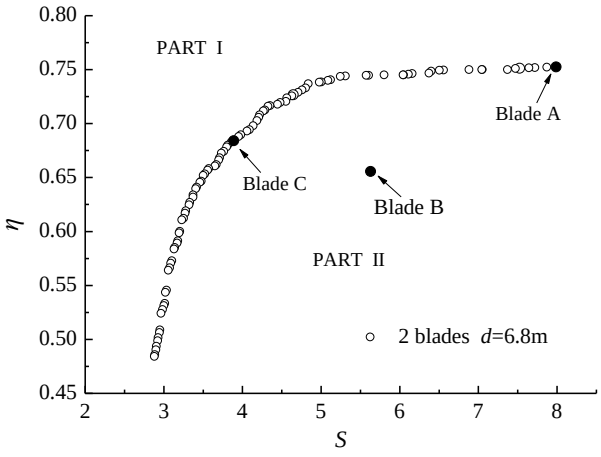

Fig. 7. Pareto-optimal solution of a 6.8-meter propeller with 2 blades

To explain the Pareto optimal solution set better, three blades marked in Fig. 7 are further analyzed. Blade A is a highly efficient propeller under the power and thrust constraints, it has the most reasonable speed triangle distribution from the propeller root to tip. Blade B is a result in the feasible solution region, and the unreasonable distribution of the chord length and pitch angle lead to the relatively low efficiency compared with the blade on the Pareto Frontier under the same blade area conditions.

On the other hand, although the efficiency of the blade C reduces by about 9% compared with blade A, the change of blade area shows a more significant decline of 47%.

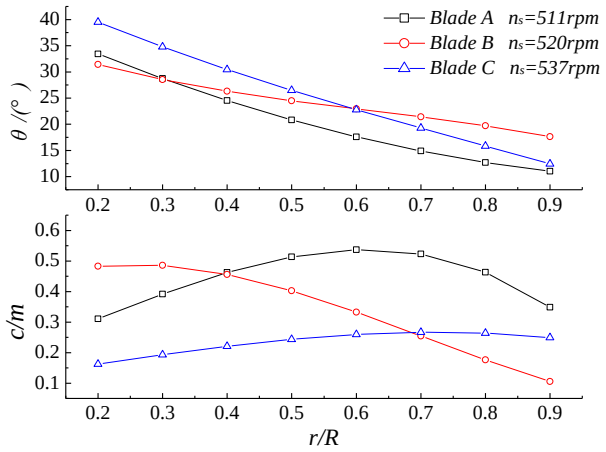

Fig. 8. Chord and pitch angle distributions of blades A, B and C

Through comparing the geometries and operating speed of blades A, B and C shown in Fig. 8.

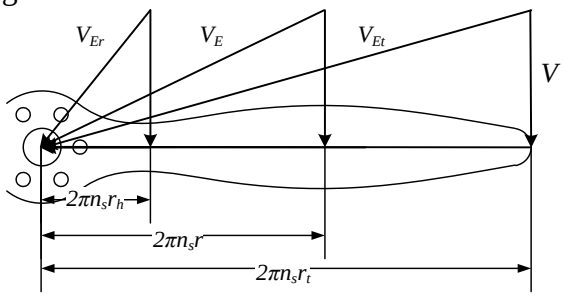

Fig. 9. Speed triangle along the blade

The high altitude propeller can't always meet these conditions from propeller root to tip, because the rotational speed of each airfoil section are quite different shown in Fig. 9. The speed triangle distribution of Blade A is more reasonable, thus it has the highest aerodynamic efficiency among the three blades. Moreover, it can be seen that, some of the propeller efficiency is sacrificed to achieve light weight, and the reduction of chord length and increase of pitch angle need to change by some discipline to maintain the speed triangle at its highly efficient operation region. Moreover, the rotational speed of propeller with small blade area is increased to meet the requirements of the absorbed power.

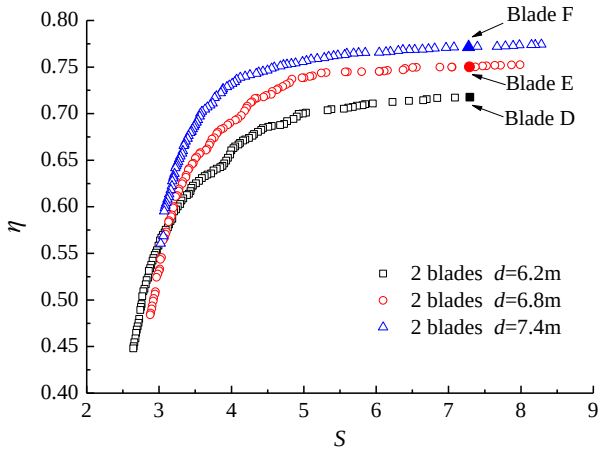

Fig. 10. Pareto-optimal solutions of two-bladed propellers with different diameters

Fig. 10 presents the Pareto-optimal solutions of two-bladed propellers with different diameters. It can be seen that the propeller with large diameter has a higher aerodynamic efficiency under the condition of the same surface area. This is because the propeller blade can be regarded as the wing model with a certain aspect ratio, and larger aspect ratio helps to reduce the induced drag and increase the lift-drag ratio. Consequently, high efficiency of propeller is seen to favor larger diameter and smaller chord length shown in Fig. 11, while smaller propeller need higher rotational speed and pitch angle to offset the bad effect on propeller efficiency and assure adequate absorbed power. Besides that, the blade surface area of large propellers is obvious smaller under the same conditions of efficiency, which is caused by the fact that the increase of chord length has a greater impact on the surface area of the propeller than the increase of the diameter. This indicates that the increase in propeller's diameter brings more benefits, whether from the aspect of the blade area or efficiency.

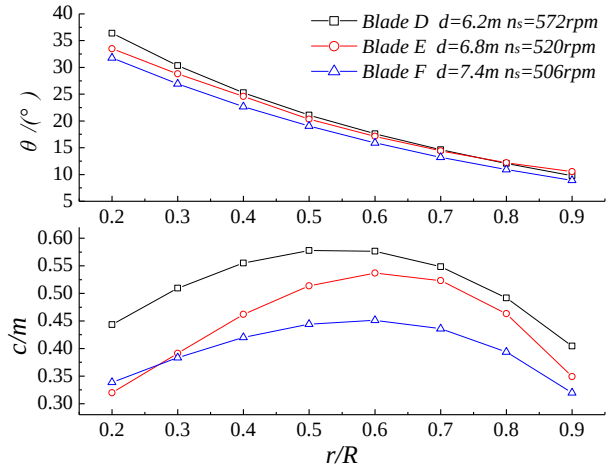

Fig.11. Chord and pitch angle of blades D, E and F

However, it should be noted that the propeller is a kind of slender body which will lead to many difficulties of the propeller's structure and manufacture. The force acted on the whole propeller is integrated by section thrust, circumferential force and centrifugal force of each blade element, which would generate deformation including extension, torsion and bending, and even structural damage if the propeller is very long and thin.

5 Comparison of experiment and calculation

In the practical engineering applications, designers have to make the decision under different working conditions and consider the tradeoff among various factors to attain a high performance and light weight design. In this project, the important requirement for the HAA propulsion system is to achieve the propeller efficiency of more than 70% at design point. To this end, the two-bladed propeller with 6.8 meters diameter is selected as the final design for the HAA. Fig. 12 presents the geometry of the 6.8-meters optimized propeller.

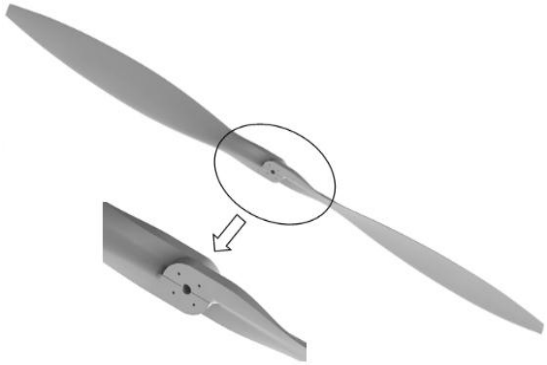

Fig. 12. Geometry of the optimal propeller

The wind tunnel test of scale model need to follow this similitude to ensure valid results [18]. However, the Reynolds number of high altitude propeller is very low because of the low atmospheric density of stratosphere, this has a great impact on the aerodynamics of the propeller blade. Therefore, the main similarity criteria required here are the advance ratio and Reynolds number, which are defined as below.

$$\begin{cases} (\mathrm{Re})_{\mathrm{model}} = (\mathrm{Re})_{\mathrm{prototype}} = (\dfrac{\rho V c}{\mu})_{\mathrm{model}} = (\dfrac{\rho V c}{\mu})_{\mathrm{prototype}} \\ (\lambda)_{\mathrm{model}} = (\lambda)_{\mathrm{prototype}} = (\dfrac{V}{n_s d})_{\mathrm{model}} = (\dfrac{V}{n_s d})_{\mathrm{prototype}} \end{cases} \tag{20}$$

Then the scaling laws between the prototype and model can be formulated as

$$d_r = \frac{c_m}{c_p} = \frac{d_m}{d_p} \tag{21}$$

$$n_r = \frac{n_{sm}}{n_{sp}} = \frac{\rho_p \mu_m d_p^2}{\rho_m \mu_p d_m^2} = \frac{\nu_r}{d_r^2} \tag{22}$$

$$V_r = \frac{V_m}{V_p} = \frac{\rho_p \mu_m d_p}{\rho_m \mu_p d_m} = \frac{\nu_r}{d_r} \tag{23}$$

According to the scaling laws, the associated parameters of the prototype and the model at design point is introduced in Table 3. This wind tunnel test was conducted in the NF-3 low speed wind tunnel at Northwestern Polytechnical University of China. The scaled propeller model is driven by a converter motor, experimental data are measured by a six component cassette strain gauge balance and other equipment, shown in Fig. 13.

Table 3. The associated parameters of the propeller prototype and model

Parameters	prototype	model
Flight altitude, km	20	0
Air density, kg/m ^{3}	0.0889	1.2250
Air dynamic viscosity, Pa s	1.4216	1.7894
Diameter, m	6.8	1
Wind speed, m/s	20	12.4
Rotational speed, rpm	510	2154
Reynolds number(r/R=0.75)	62500	62500
Advance ratio	0.346	0.346

Fig. 13. Wind tunnel test

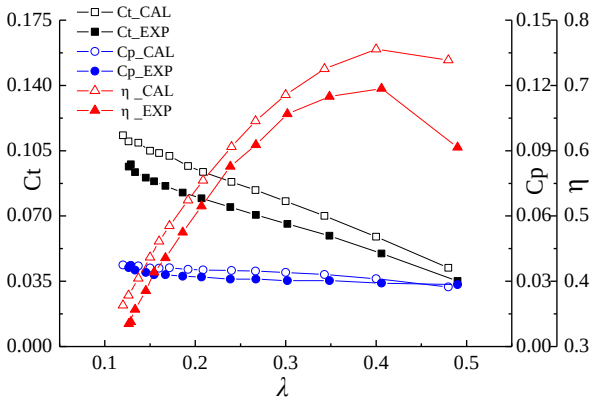

(a) Performance at wind velocity of 8m/s

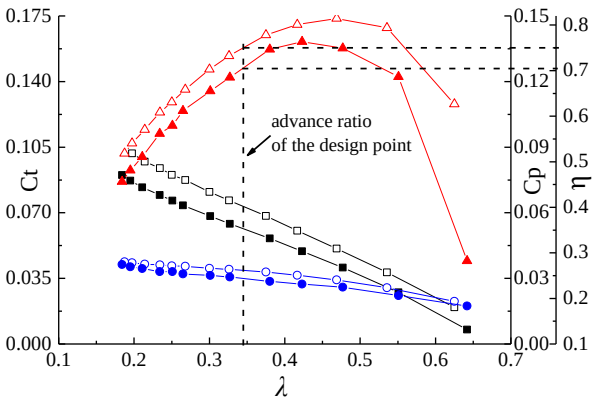

(b) Performance at wind velocity of 12.5m/s

Fig. 14. Comparisons of propeller performance between experiment and calculation

As shown in Fig. 14, the results obtained from the wind tunnel test are in fair agreement with the calculation results of the optimal propeller at different wind velocities. The vortex theory predicts a slightly bigger power coefficient than experimental data, but the maximum efficiency is estimated to be about 8% higher than the test values. This is related to the method's over prediction of the thrust coefficient at high advance ratios.

The efficiency of the 1-meter propeller model is about 70.5% at the advance ratio of 0.346, shown in Fig. 22 (b), and is relatively lower than the calculated result of 75.2% at the design point. This indicates that the optimized propeller can satisfy the design requirements of the HAA propulsion system.

6 Conclusions

In this paper, a multi-objective optimization design of propeller for HAA is conducted based on the vortex theory and the NSGA-II algorithm. The variation effects of the different design parameters on high altitude propeller's efficiency and weight are discussed in detail based on the Pareto-optimal solutions. The scaled model of the optimized propeller was tested in NF-3 wind tunnel according to the scaling laws. Results obtained from the experiment agree well with those of the numerical calculations, it verifies the validity of the optimization model, and demonstrate that the designed propeller is able to satisfy the requirements of the HAA propulsion system and operate well in the stratosphere.

References

[1] Colozza A and Dolce J L. High-altitude, long-endurance airships for coastal surveillance. NASA/TM-2005-213427, 2005.

[2] Ilieva G, Páscoa J, Dumas A, and Trancossi M. A critical review of propulsion concepts for modern airships. *Open Engineering*, Vol. 2, No. 2, pp 189-200, 2012

[3] Colozza A, and Dolce J. Initial feasibility assessment of a high altitude long endurance airship. NASA/CR-2003-212724, 2003.

[4] Dumas A., Trancossi M., Madonia M., and Giuliani I. Multibody Advanced Airship for Transport. SAE Technical Paper 2011-01-2786, 2011.

[5] Pancotti A. An overview of advanced concepts for near-space systems. AIAA Paper 2009-4805, 2009.

[6] Adkins, C. N., and Liebeck, R. H., "Design of optimum propellers. *Journal of Propulsion and Power*, Vol. 10, No. 5, pp 676-682, 1994.

[7] Colozza A. High altitude propeller design and analysis overview. NASA/CR 98-208520, 1998.

[8] Monk J S. A propeller design and analysis capability evaluation for high altitude application. Master

Degree Thesis, University of the Witwatersrand, Johannesburg, 2011.

[9] Morgado J, Abdollahzadeh M, Silvestre M A R and Páscoa J C. High altitude propeller design and analysis. *Aerospace Science and Technology*, Vol. 45, pp 398-407, 2015.

[10] Wang Quan, Chen Jin, Guo Xiaofeng, et al. Optimal design of a new wind turbine blade based on performance and light weight. *Acta Aerodynamica Sinica*, Vol. 32, No. 1, pp 77-84, 2014.

[11] McCormick B W. *Aerodynamics, aeronautics, and flight mechanics (Vol. 2)*. John Wiley and Sons, Wiley, New York, 1995.

[12] Drela M. XFOIL: An analysis and design system for low Reynolds number airfoils. *Low Reynolds number aerodynamics*, Springer Berlin Heidelberg, 1989.

[13] Morgado J, Vizinho R, Silvestre M A R, et al. XFOIL vs CFD performance predictions for high lift low Reynolds number airfoils. *Aerospace Science and Technology*, Vol. 52, pp 207-214, 2016.

[14] Benini E, Toffolo A. Optimal design of horizontal-axis wind turbines using blade-element theory and evolutionary computation. *Journal of Solar Energy Engineering*, Vol. 124, No. 4, pp 357-363, 2002.

[15] Colozza A J. APEX 3D propeller test preliminary design. NASA/CR-2002-211866, 2002.

[16] Deb K, Pratap A, Agarwal S, et al. A fast and elitist multiobjective genetic algorithm: NSGA-II. *Evolutionary Computation, IEEE Transactions on*, Vol. 6, No. 2, pp 182-197, 2002.

[17] Huang B, Buckley B, Kechadi T M. Multi-objective feature selection by using NSGA-II for customer churn prediction in telecommunications. *Expert Systems with Applications*, Vol. 37, No. 5, pp 3638-3646, 2010.

[18] Liu P Q, Ma R, Duan Z Z and Ma L C. Experiment study of light-weight, high-efficiency propeller of stratospheric airships in ground wind tunnel. *Journal of Aerospace Power*, Vol. 26, No. 8, pp. 1775-1781, 2011.

Copyright Statement